

# Three-dimensional study of fatigue crack propagation using synchrotron X-ray microtomography

N. Limodin<sup>1\*</sup>, J.Y. Buffière<sup>1</sup>, J. Réthoré<sup>1</sup>, F. Hild<sup>2</sup>, S. Roux<sup>2</sup>, W. Ludwig<sup>1,3</sup>  
<sup>1</sup> INSA Lyon, Villeurbanne, France; <sup>2</sup> ENS de Cachan, Cachan, France; <sup>3</sup> ESRF, Grenoble, France

## 1 INTRODUCTION

Synchrotron X-ray microtomography imaging was used to study crack propagation taking into account the 3D nature of the crack morphology. A small loading device, which is directly mounted on the tomography set-up, enabled for in-situ loading and cycling of pre-cracked specimens. Scans were acquired during loading and unloading of the specimen to provide 3D images of the bulk in the vicinity of the crack at different fractions of the total propagation life. The tomographic images were subsequently treated by 3D Digital Image Correlation (DIC). DIC has already been used to measure Crack Opening Displacement (COD) and to estimate the corresponding stress intensity factor (SIF) value at the specimen surface [1]. However, up to now it has been performed in 2D only because 3D extensions of DIC are still new [2]. In the present work, the application of 3D-DIC to tomographic data allowed rapid retrieving of the displacement field in the bulk of the cracked specimen. From this displacement field, both the crack geometry and COD could be obtained. The above mentioned method was applied to specimens cut from different regions of larger fatigue pre-cracked samples made of nodular graphite cast iron to study the influence of the stress state in the larger sample on further crack growth in the smaller specimens.

## 2 MATERIAL AND METHODS

The studied material is a ferritic nodular graphite cast iron (3.65 wt% C, 3.2 wt% Si, 0.04 wt% Mg, <0.1 wt% Mn, <0.005 wt% S, 0.02 wt% P). After casting and heat treatment, the microstructure consists of a ferritic matrix with a homogeneous distribution of nearly spherical graphite nodules having an average diameter of 45  $\mu\text{m}$  and a volume fraction of 14%. Young's modulus, yield stress and Poisson's ratio are equal to 175 GPa, 315 MPa, and 0.27, respectively. More details can be found in Ref. [3]. Carbon (nodules) and iron (matrix) have atomic numbers that are different enough to give a strong X-ray attenuation contrast. The

---

\* MATEIS, CNRS UMR 5510, INSA Lyon, St Exupéry /3e, F-69621 Villeurbanne, France  
Tel: (33) 4 72 43 71 76  
E-mail: nathalie.limodin@insa-lyon.fr

nodules are thus easily imaged by tomography and can be used as natural markers for image correlation. Notched specimens with a  $6 \times 4$ -mm cross-section were pre-cracked in fatigue at a stress ratio of 0.1. The specimen faces were mirror polished to monitor crack growth with an optical travelling microscope. A load-shedding technique was used to maintain a value of the maximum Stress Intensity Factor (SIF) less than  $12.8 \text{ MPa}\sqrt{\text{m}}$  to make sure that the plastic zone size is less than  $200 \mu\text{m}$  at the crack tip (in plane strain). Fatigue cycling was stopped as soon as the crack had reached 1.5 mm in length. For the tomography experiment, two smaller dog-bone specimens with a square cross-section of  $1.6 \times 1.6$  mm were spark cut inside two larger samples so that they enclose only a part of the crack tip. One small specimen was cut from one flat side of the larger sample so that one edge of the small specimen contains the crack tip at the former surface (close to a plane stress condition) while the other edge contains the crack tip that was at the centre of the larger specimen (close to plane strain). Another small specimen was cut from the mid-thickness of the large specimen (close to pure plane strain). These specimens will be referred to as side specimen and centre specimen hereafter.

The tomography experiments were performed on the ID19 beam line at the European Synchrotron radiation Facility (ESRF) in Grenoble, France. A monochromatic X-Ray beam ( $\Delta\lambda/\lambda = 10^{-2}$ ) having a photon energy of 60 keV traverses the sample (Fig. 1) giving an incident-to-transmitted intensity ratio of about 10%. To obtain a complete scan of the specimen cross-section in the vicinity of the crack, six hundred radiographs were taken while the sample was rotating over  $180^\circ$  along its vertical axis; the scan time amounts to 42 minutes. A FReLoN (Fast Readout Low Noise) 14-bit CCD camera with a  $2048 \times 2048$  pixel chip was used. A specially designed fatigue machine allowed for in-situ cycling and loading of the specimen. A PMMA tube, almost transparent to X-ray, is used as a load rig. The machine was directly mounted on the rotating stage (Fig. 1) of the beam line. Firstly, the specimen was progressively loaded to a maximum load, which is expected to result in a maximum stress intensity factor slightly smaller than the maximum value used in fatigue pre-cracking, and scans were acquired for different loading steps up to this maximum load. The specimen was then cycled at a stress ratio of 0.1 under constant amplitude to propagate the crack and scans were recorded at various fractions of the fatigue life. Reconstruction of the tomographic data was performed with a conventional filtered back-projection algorithm. It provides a 3D image with a greyscale colormap that is proportional to the local X-ray attenuation coefficient. A final region of interest of size  $340 \times 340 \times 512$  voxels with a voxel size of  $5.06 \mu\text{m}$  was then focused on the crack to limit data size.

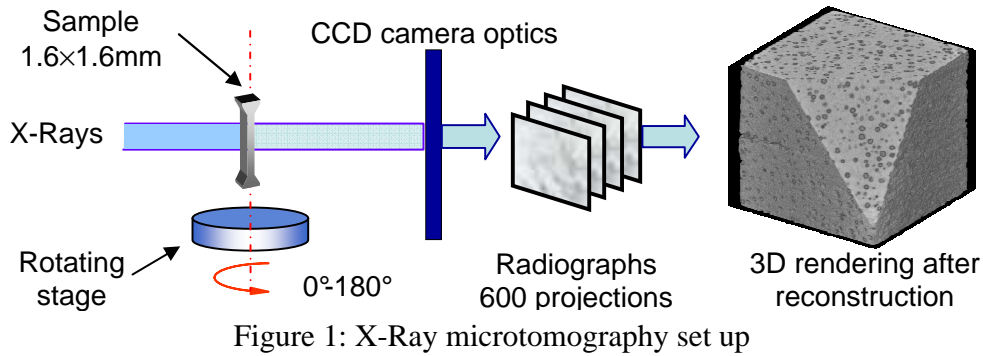


Figure 1: X-Ray microtomography set up

DIC is a well established technique for computing displacement and strains at the specimen surface. In 3D, the same principle applies. Displacement fields are measured between a pair of images (here 3D reconstructed scans) of the same specimen at different loads. Images in grey level are characterized by  $f$  and  $g$ , their respective grey level valued function of pixel coordinates,  $\mathbf{x}$ . The displacement field is obtained, using the so-called optical flow conservation, so that the image of the loaded sample,  $g$ , (i.e. the “deformed image”) is matched to the reference image,  $f$ , when voxel location,  $\mathbf{x}$ , is corrected for by the displacement field,  $\mathbf{u}$

$$f(\mathbf{x}) = g(\mathbf{x} + \mathbf{u}(\mathbf{x})) \quad (1)$$

A correlation algorithm based on a finite element kinematics [2] was used. The image acquired at minimum load in the first cycle, i.e. at 14 and 24N for the side and centre specimens respectively, was used as the reference image, and correlation was sought between this reference image and the deformed image obtained at higher loads. A region of interest (ROI) of  $288 \times 288 \times 288$  voxels was centred on the original tomographic image. Eight-node cubic elements with an isotropic size of 16 voxels were chosen to mesh the ROI. Inside the cracked specimen, the presence of the crack discontinuity avoids matching the reference image to the corrected image. The difference between both images is the residual error map that gives invaluable information about the crack geometry as will be shown hereafter.

### 3 RESULTS

In the tomographic images, the apparent crack tip position can be measured via simple visual inspection using ImageJ software [4]. A plug-in allows for retrieving the coordinates of the pixel that is manually selected as the crack tip at each slice through the sample thickness. This enables one to detect variations of the crack front position with number of cycles for the side specimen (Fig. 2a) and the centre specimen (Fig. 2b). The crack lengths measured at the specimen

surface with an optical microscope, at a better resolution than the tomographic images, are also plotted for comparison purposes. A difference in propagation behaviour is clearly visible between the two samples. On one hand, for the centre specimen, a crack advance is visible after only 2,000 cycles (“257N\_2k”) on the right hand side in Fig. 2b while the crack length on the other side remained almost unchanged until 3,000 cycles (“250N\_3k”) after which it grows at the same rate as other points along the crack front. On the other hand, in the side specimen, the crack remained arrested from the first cycle (“228N”) to 40,000 cycles (“187N\_40k”) with a crack tip position that is close to that initially observed with a microscope (Fig. 2a). A crack advance finally appeared after 45,000 cycles (“186N\_45k”) with a crack growth rate that seems uniform along the crack front.

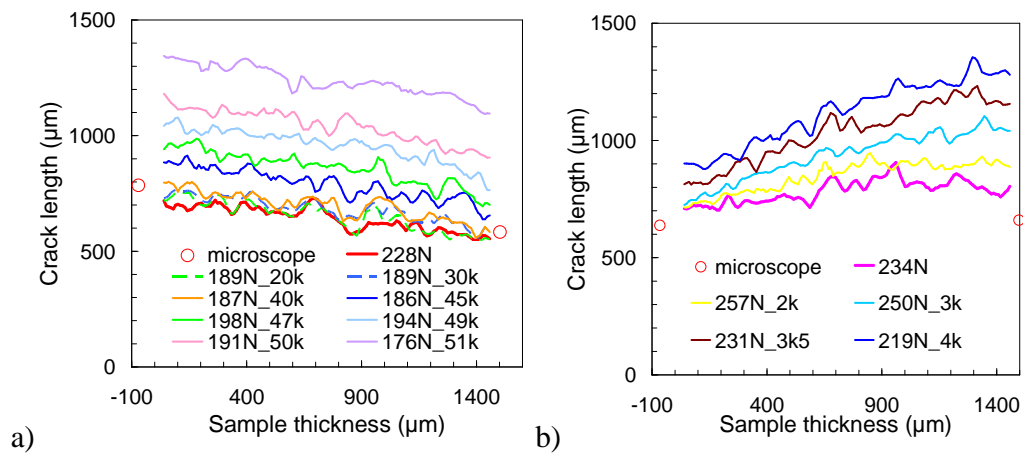


Figure 2: Crack tip position in the (a) side specimen and (b) centre specimen under maximum load at different numbers of cycles

Usually, tomographic images are thresholded to obtain a 3D rendering of the crack. However, in cast iron, the similarity of grey value between the crack and the nodules makes it impossible to visualize the crack alone. Therefore, the residual error map from DIC was thresholded using a 3D region growing algorithm to extract the voxels that belong to the crack from those corresponding to noise [5]. Figure 3 shows the crack geometries in the side and centre specimens after some propagation has occurred. The crack extent observed from the thresholded residual map matched the crack tip positions shown in Fig. 2 as soon as the crack tip is open enough, i.e. after 20,000 cycles for the side specimen and after 2,000 cycles for the centre specimen. The crack in the side specimen (Fig. 3a) is macroscopically flat with a slightly dissymmetric front that has maintained its shape during crack growth; dissymmetry can probably be attributed to a crack tunnelling effect with a crack that is longer on the side that was predominantly under plane strain condition in the larger pre-cracked specimen.

The crack surface in the centre specimen shows a step on the right hand side that has been inherited from the larger fatigue specimen (see detail of the crack

surface highlighted in red in Fig. 3b). The crack on one side of the specimen has slowly departed from its mode I crack plane before reaching another straight crack path 600  $\mu\text{m}$  away from the notch and about 150  $\mu\text{m}$  above the main crack path. Reasons for this crack branching could not be inferred from surface observations and the microstructure (graphite nodule distribution) observed in the reconstructed image does not show any particular feature that may explain crack arrest. Due to this retardation effect, the initially symmetric and almost straight crack front shown in Fig. 2b has become dissymmetric during in situ cycling with a crack that is smaller on the right hand side in Fig. 3b where it was initially stopped.

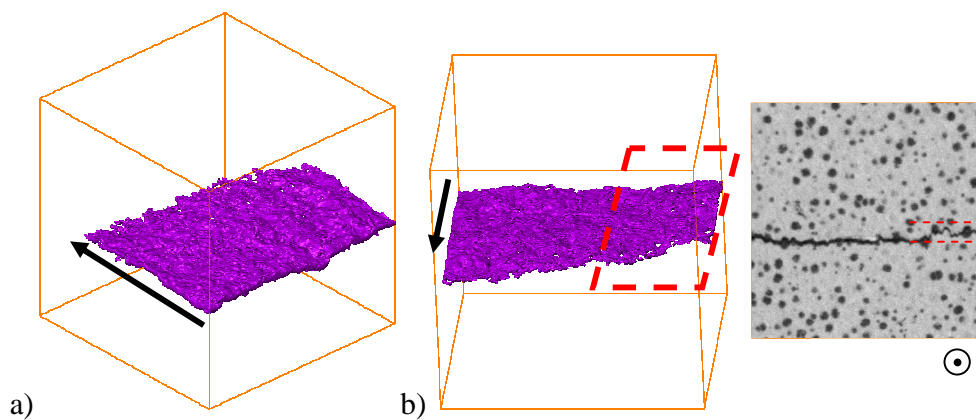


Figure 3: Crack geometry in (a) the side specimen at 194N after 49,000 cycles and (b) in the centre specimen at 250N after 3,000 cycles (direction of crack growth is indicated by an arrow); a slice normal to the crack plane is extracted from the tomographic image to highlight the step in the crack path

Image correlation provided the full displacement fields in the bulk of the specimen. Figure 4a shows an example of the displacement field,  $U_z$ , along the loading axis at the maximum load of the first loading cycle, in the centre specimen. The discontinuity due to the crack presence enables for the study of the mode I crack opening at a local scale. In Fig. 4b, a gradient of  $U_z$  along a line indicated in blue in Fig. 4a is plotted for a position close to the crack mouth. The  $U_z$  profile appears smooth and continuous away from the crack. Thus, the displacement jump on the crack surface, or COD, can be estimated from the difference between two slices on either side of the crack discontinuity in the  $U_z$  field. The resulting COD map is plotted in the specimen cross-section in Fig. 4c; areas in light greys correspond to maximum opening. From this map, COD profiles are plotted at various locations in the sample thickness, for example along the red lines drawn in Fig. 4c, as a function of the distance to the crack mouth. Assuming a linear elastic behaviour, the crack tip displacement field in Mode I is known [6] and the SIF (Eq. (2)) is computed directly from the best fitting curve in Fig. 4d

$$u_z(\pi) - u_z(-\pi) = \frac{8K_I}{E} \sqrt{\frac{r}{2\pi}} = COD \text{ with } r, \text{ the distance to the crack tip} \quad (2)$$

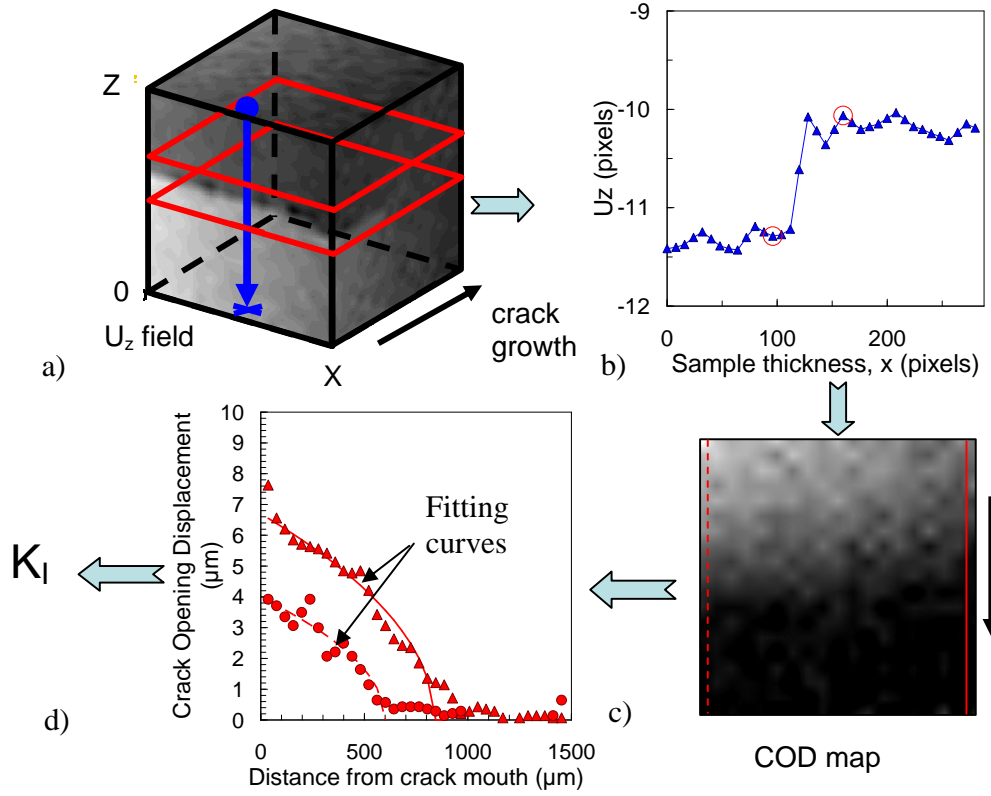


Figure 4: Determination of the (c) COD map in the specimen cross-section using the (b) discontinuity in the (a) 3D displacement field  $U_z$  and subsequent  $K_I$  computation from the (d) COD profile along the crack growth direction (the arrow indicates the crack growth direction)

A 2D map of COD values is shown in Fig. 5 together with the crack tip position reported in Fig. 2. In the side specimen (Fig. 5a), the crack tip opening was less than 0.3 voxel at the maximum load of the first cycle so that it can be considered closed. At 20,000 and 30,000 cycles, it has increased up to 0.4 voxel locally and at 40,000 cycles, it has reached an almost uniform value of 0.4 voxel while no significant growth has occurred. At 45,000 cycles and after, a further increase in COD occurred concomitantly with crack propagation.

Figure 5b shows the COD change with the number of cycles in the centre specimen from the first loading cycle to 3,000 cycles. At the first cycle, the crack was locally closed, i.e. with an opening less than 0.1 voxel, at the tip on the right hand side of the map whereas the opening amounted to 0.4 voxel on the left hand

side. At 2,000 cycles, the crack has visibly grown on the left hand side while the crack tip position remained the same on the right hand side. Meanwhile, as the crack propagated on the left hand side, the COD increased on both sides of the specimen with still a much larger value on the side of the growing crack. After 3,000 cycles, the COD was about 2 voxels on the left and 1.4 voxel on the right hand side. The crack began to grow uniformly after 3,000 cycles.

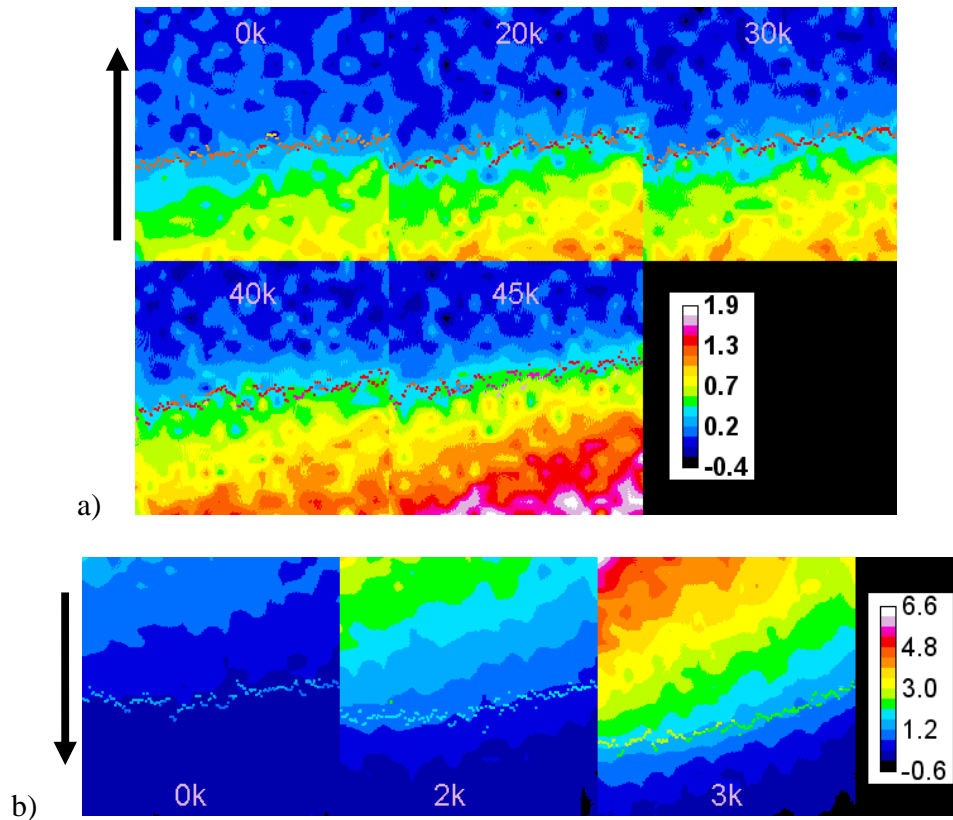


Figure 5: COD maps at maximum loads for various numbers of cycles in (a) the side specimen and (b) the centre specimen (colormap in voxels)

#### 4 DISCUSSION

Specimens with different stress state history at their surface have shown different behaviours under fatigue cycling conditions that were designed to induce similar  $\Delta K$  values.

In the side specimen, the crack tip changes reported in Fig. 2a remain in the range of the crack length measured optically before tomography between 0 and 40,000 cycles of fatigue. Thus, the crack can be considered arrested and reasons for this

retardation are likely to be due to crack closure at the tip. The COD maps in Fig. 5a remain fairly unchanged from the initial cycle up to 30,000 cycles with a value at the crack tip that increases very slightly. Only after 40,000 cycles does the COD increase noticeably (both at the tip and crack mouth) as compared to previous maps. This increase of COD results into an increase of the corresponding  $K_I$  values obtained from COD maps, namely, at the first loading cycle, the SIF ranges from 7.6 to 5.5 MPa $\sqrt{m}$  for, respectively, the long and short crack side then, this range rises up to 10.1 to 11.8 MPa $\sqrt{m}$  at 40,000 cycles. Ogawa [7] reported values for the opening SIF,  $K_{op}$ , that are ranging from 6.5 to 9.5 MPa $\sqrt{m}$  for a similar material. The SIF values computed for the arrested crack are thus consistent with a crack that remained closed. Then, noticeable crack growth at 45,000 cycles results into a further larger increase in  $K_I$  as expected (constant amplitude cycling). Initial crack closure might be attributed to the plastic zone size. Due to the small thickness of the tomography sample, it is possible that a large portion of the crack front is affected by the plastic zone size in plane stress inherited from the larger specimen. Once crack opening has reached a value high enough, the crack propagates at a rate in accordance with the  $da/dN-\Delta K$  curve reported in Ref. [8].

The crack in the centre specimen that has assumingly a plastic zone corresponding to plane strain condition all along its front was observed to propagate immediately when submitted to fatigue cycling again. This suggests that crack closure in plane strain is very small so that when submitted to conditions close to those used in pre-cracking, the crack opens immediately and almost the full  $\Delta K$  range is available for crack growth. The measured values of  $K_I$  at maximum load are 12.7 and 8.9 MPa $\sqrt{m}$ , respectively on the growing and arrested crack side for the first loading cycle. Note that the 8.9 MPa $\sqrt{m}$  value is in the range of the  $K_{op}$  value in Ref. [7]. Although plasticity induced crack closure is not expected to be important in plane strain conditions, close examination of the COD maps reveals that the crack seems partially closed on one side (Fig. 5b). The crack geometry observed in Fig. 3b shows that the area where the crack is closed at its tip and remains arrested during 3,000 cycles corresponds to a bifurcation of the crack path. A step of constant height from crack mouth to tip is visible on the right hand side of Fig. 3b. This crack branching could have induced crack retardation and subsequent roughness induced crack closure due to the presence of the asperity. The spatial resolution of the displacements fields along the  $x$  and  $y$  axis is not accurate enough to observe mixed mode loading occurrence at the asperity. However, computation of SIF along the crack front as in Ref. [5] may be able to catch such mixed mode occurrence at a local scale. After 2,000 cycles, the crack seems fully open under maximum load, i.e. at 257N, as shown on the COD maps in Fig. 5b and the corresponding  $K_I$  values of 25.9 and 20.3 MPa $\sqrt{m}$  are consistent with rapid crack growth, i.e. at a rate of about  $10^{-4}$  mm / cycle as reported in Ref. [8].

## **5 CONCLUSIONS**

Application of 3D-DIC to crack propagation data obtained with tomography enables for the study of the influence of the loading history on crack growth. Crack under initial plane strain condition was observed to propagate as soon as the cyclic loading starts. However, it was proved sensitive to the roughness of the crack path that may induce crack growth retardation. To understand the roughness influence, the method described in [5] will soon be used to retrieve the SIF values along the crack front and to check if crack asperities induce mixed mode at the crack tip. When submitted to cyclic loading with a similar  $\Delta K$  range, a crack with mixed plane stress to plane strain condition along its front was observed to remain arrested for more than 40,000 cycles. This retardation is thought to be due to plasticity induced crack closure. The combination of full 3D image analysis to visualize the crack, COD analysis and SIF computation along the crack front is the first step towards a complete understanding of 3D crack propagation knowing the crack history and geometry. Next step would be to model the crack propagation.

## **ACKNOWLEDGEMENTS**

This work was carried out in the framework of the project “PROPAVANFIS” supported by the CETIM foundation, which is gratefully acknowledged. The authors are also grateful to ESRF for providing beam time on the ID19 beam line and to all staff members of the line for their help during the experiments.

## REFERENCES

- [1] W. Mekky, P.S. Nicholson, The fracture toughness of Ni/Al<sub>2</sub>O<sub>3</sub> laminates by digital image correlation I: Experimental crack opening displacement and R-curves, *Engineering Fracture Mechanics* 73 (5) (2006) 583-592.
- [2] S. Roux, F. Hild, P. Viot, D. Bernard, Three-dimensional image correlation from X-ray computed tomography of solid foam, *Composites: Part A* 39 (8) (2008) 1253-1265.
- [3] J. Adrien. Optimisation des cycles thermiques appliqués aux fontes G.S. ferritiques vis à vis des propriétés de fatigue, Ph.D. Thesis: Institut National des Sciences Appliquées de Lyon, 2004.
- [4] <http://rsb.info.nih.gov/ij/>.
- [5] J. Rannou, N. Limodin, J. Réthoré, A. Gravouil, W. Ludwig, M.-C. Baietto-Dubourg, J.-Y. Buffière, A. Combescure, F. Hild, S. Roux, Three dimensional experimental and numerical multiscale analysis of a fatigue crack, submitted for publication.
- [6] T.L. Anderson, *Fracture Mechanics: fundamentals and applications*, 2nd ed., CRC Press, Boca Raton, Florida, 1995.
- [7] T. Ogawa, H. Kobayashi, Near-threshold fatigue crack growth and crack closure in a nodular cast iron, *Fatigue Fracture of Engineering Materials* 10 (4) (1987) 273-280.
- [8] Y. Nadot, N. Ranganathan, J. Mendez and A.S. Béranger, A study of natural cracks initiated on casting defects by crack front marking, *Scripta Materialia* 37 (5) (1997) 549-553.